IAES International Journal of Robotics and Automation (IJRA)
Vol. 14, No. 4, December 2025, pp. 399~408
ISSN: 2722-2586, DOI: 10.11591/ijra.v14i4.pp399-408

ADC-LIO: A direct LiDAR-inertial odometry method based on adaptive distortion covariance

Lixiao Yang, Youbing Feng
Ocean College, Jiangsu University of Science and Technology, Zhenjiang, China

Article Info

Article history:

Received Jan 15, 2025
Revised Nov 7, 2025
Accepted Nov 11, 2025

Keywords:

Dense mapping
Kalman smoother
Lidar inertial odometry
Sensor fusion
Simultaneous localization and mapping

ABSTRACT

Focusing on the localization challenges for robots in dynamic navigation environments, this study proposes a direct LiDAR-inertial odometry (LIO) system named ADC-LIO, which achieves robust pose estimation and accurate map reconstruction using adaptive distortion covariance. ADC-LIO is engineered to address uncertain motion patterns in autonomous mobile robots, effectively integrating LiDAR scan undistortion within the Kalman filtering update process by embedding an iterative smoothing process and a backpropagation strategy. The ADC-LIO architecture enhances point cloud accuracy, improving the system's overall performance and robustness. In addition, an adaptive covariance processing method is developed to resolve motion-induced sensing uncertainties, which calculates different covariances according to the error characteristics of the point cloud. This method enhances the constraints of high-quality point clouds, reduces the limitations on low-quality point clouds, and utilizes information more effectively. Experiments on the publicly available NTU-VIRAL dataset validate the effectiveness of ADC-LIO, which improves pose estimation accuracy and reduces absolute position errors compared to other state-of-the-art methods, including FAST-LIO, Faster-LIO, FR-LIO, and Point-LIO. The proposed ADC-LIO is an appealing odometry method that delivers accurate, real-time, and reliable tracking and map-building results, posing a practical solution for robotic applications in structured indoor and GPS-denied outdoor environments.

This is an open access article under the CC BY-SA license.

Corresponding Author:

Youbing Feng
Ocean College, Jiangsu University of Science and Technology
Zhenjiang, China
Email: yzfyb@just.edu.cn

1. INTRODUCTION

Simultaneous localization and mapping (SLAM) technology is advancing rapidly in today's rapidly evolving robotic sector. As a cornerstone of autonomous robot navigation, SLAM directly enables critical robotic functionalities, including environment perception, path planning, and obstacle avoidance. Vision-based SLAM affords high location accuracy and is commonly employed in mobile robots owing to its lightweight and low cost [1]–[4]. Nevertheless, algorithms that explore data from the visual domain, while providing high-resolution RGB data, do not capture depth directly and require substantial computational effort to recover the 3D scene necessary for motion planning. Opposing vision-based SLAM, light detection, and ranging (LiDAR) sensors afford enhanced LiDAR-odometry (LO) capabilities [5] and thus have become an integral part of self-driving cars [6], [7], unmanned aerial vehicles (UAVs) [8], [9], and other mobile robots. Their high accuracy and ability to directly acquire 3D environmental information make them indispensable for robotic systems operating in GPS-denied or geometrically complex workspaces. The effectiveness of the LO system primarily depends on its precision, stability, and operational efficiency.

However, processing LiDAR data requires a large amount of computational resources, especially in high-speed motion or complex environments, which puts higher demands on real-time performance and accuracy. To address this challenge, architectures that fuse LiDAR and inertial measurement units (IMUs), namely LiDAR-inertial odometry (LIO), have emerged [10], [11].

LIO provides a critical advantage for autonomous robots navigating in dynamic environments by synergizing LiDAR's precise geometry sensing with IMU's high-frequency motion tracking. This fusion strategy enhances the system's accuracy and reliability while reducing the computational burden through the use of intelligent algorithms, thereby enabling real-time processing. Various methods have been proposed to enhance registration accuracy, such as employing more precise probabilistic map representations [12], applying finer LiDAR point segmentation [13], [14] or selecting more informative points for registration [15]. Additionally, several methods enhance accuracy by compensating for motion distortion in LiDAR data [16], [17]. FAST-LIO [18] and FAST-LIO2 [19], as representative LIO methods, achieve highly accurate state estimation while maintaining computational efficiency through tightly coupled iterative Kalman filters. FAST-LIO2 further optimizes the data processing flow by introducing the incremental k-dimensional tree (ikd-Tree) data structure for dynamic map updating and efficient nearest neighbor search, significantly improving the utility and flexibility of an LIO system. Faster-LIO [20] extends FAST-LIO2 by replacing the ikd-Tree with iVox and optimizing the code logic to achieve faster LIO processing. In [21], the authors introduce a point-by-point (point-wise) LIO framework that fuses LiDAR points during sampling without accumulating them in the frame. Removing point accumulation eliminates intra-frame motion distortion, allowing for high odometry output and build-up updates at near-point sampling rates. This enables the system to track swift motion and simultaneously support incremental updating and dynamic rebalancing, allowing odometry and map-building frequencies of up to 100 Hz despite limited computational resources. The work in [22] proposes a tightly coupled, iterative error state Kalman smoothing (ESKS) framework for state estimation, which achieves robust tracking and location in violent motion scenarios by smoothing the position in the degraded direction of the current subframe. This smoothing process is completed by combining the history and constraint information on future subframes. Nevertheless, current LIO systems still face several challenges. For instance, the IMU attempts to correct point cloud data distortion by integrating positional information. However, these errors are challenging to eliminate due to sensor noise, drift, and other dynamic influences during the integration process of the IMU. In robotic applications where sustained accuracy over long missions is crucial, motion distortions often persist in the point cloud, limiting further improvements in the LIO system's accuracy.

To address this issue, this paper introduces an enhanced method named iterated backward propagation, which combines iterative Kalman smoothing with backpropagation to reduce distortion errors in the LiDAR scan. This innovation focuses on the motion distortion patterns observed in wheeled robots during abrupt acceleration/deceleration and UAVs during aerial rotations. The approach iteratively refines the LiDAR scan's undistortion process, thereby improving the accuracy and robustness of the system and leading to more precise pose estimation and overall enhanced performance. Moreover, existing LIO systems typically assume uniform confidence levels for all points in the LiDAR scan when formulating the observation equations. However, due to the motion of the LiDAR sensor, different points in the scan exhibit varying residual distortion errors. Therefore, an adaptive distortion covariance calculation method is developed to weigh the points with different distortion uncertainty during the Kalman update process. This method enhances the weighting of high-quality points, reduces the influence of low-quality points, and ensures more efficient utilization of the available information, ultimately improving the system's overall performance and robustness. The proposed method's effectiveness is verified by qualitative and quantitative experiments on the publicly available NTU-VIRAL dataset [23]. The experimental results demonstrate that, compared with FAST-LIO2, the proposed algorithm improves average accuracy and exhibits higher refinement in the build effect.

The remainder of this paper is organized as follows. Section 2 introduces and analyzes the proposed method. Section 3 presents the experimental findings on the NTU-VIRAL dataset, and section 4 concludes this work.

2. METHODOLOGY

2.1. Framework overview

The proposed ADC-LIO system is illustrated in Figure 1. It is designed to process high-frequency (100 Hz) IMU data and relatively low-frequency (10 Hz) LiDAR scans, outputting odometry information at the frequency of the LiDAR scan. ADC-LIO relies on an iterative error Kalman filter framework, where IMU data is used for Kalman prediction and point cloud data is used for the Kalman update process to maintain pose estimation consistency under dynamic robotic motion. During the iterative update procedure, Iterated Backward Propagation further enhances the point cloud undistortion effect, which is critical for robots operating in high-acceleration scenarios. Additionally, an adaptive distortion covariance calculation balances

the constraints of high-precision points and reduces the influence of erroneous points, thereby improving the overall performance and accuracy of the system.

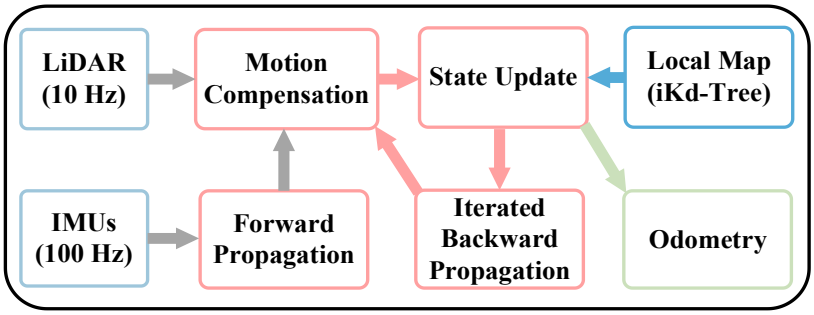

Figure 1. System overview of ADC-LIO

2.2. Forward propagation

Let the state variables of the system be $[{}^{G}R_I, {}^{G}p_i, {}^{G}v_I, b_a, b_\omega, {}^{G}g]$, where ${}^{G}p_i$, ${}^{G}R_I$, and ${}^{G}v_I$ denote the IMU position, rotation, and speed in the global reference frame, ${}^{G}g$ is the gravity vector in the global reference frame, b_a and b_ω are the IMU biases, modeled as a random walk process. The forward transfer of the IMU is computed based on the discrete IMU motion model. The first IMU frame is defined as the global reference frame in this process. The kinematic model for forward propagation is computed using the kinematic model below, which propagates the IMU's state from the initial frame through subsequent time steps.

$$
\begin{aligned}
&{}^{G}\dot{R}_I = {}^{G}R_I[\omega_m - b_\omega - n_\omega]_\wedge,\ {}^{G}\dot{p}_I = {}^{G}v_I \\
&{}^{G}\dot{v}_I = {}^{G}R_I(a_m - b_a - n_a) + {}^{G}g \\
&\dot{b}_\omega = n_{b\omega}, \dot{b}_a = n_{ba} \\
&{}^{G}\dot{g} = 0,\ {}^{I}\dot{R}_L = 0,\ {}^{I}\dot{p}_L = 0
\end{aligned} \tag{1}
$$

where a_m and ω_m are IMU measurements, n_a and n_ω represents the noise measurement of a_m and ω_m, respectively, and $[a]_\wedge$ is the skew-symmetric cross product matrix of vector $a \in R^3$.

2.3. Iterative backward propagation

Unlike methods such as FAST-LIO2, which compensate for distortion with a single forward and backward propagation, this paper introduces an iterative backward propagation scheme integrated with Kalman smoothing. This approach effectively combines point cloud distortion removal with state updating, enhancing both processes. Specifically, smoothing the IMU position after each state update provides more accurate LiDAR coordinates for the next backward propagation iteration, further reducing residual distortions. Figure 2 illustrates the iterative process of the proposed scheme, which progressively refines the system's performance through backward propagation, state updating, and Kalman smoothing. These modules are analyzed below.

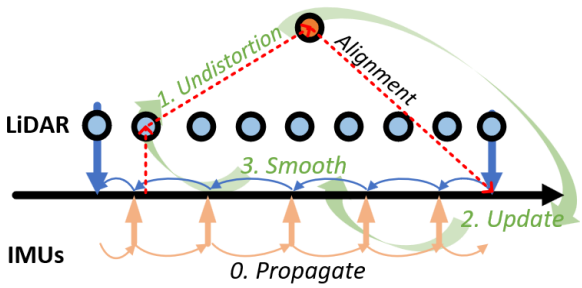

Figure 2. Iterative backward propagation, state updating, and Kalman smoothing. Smoothing the IMU position after each state update enhances the accuracy of the LiDAR coordinates for the next backward propagation iteration, thereby reducing residual distortions

2.3.1. Motion compensation

The LiDAR scan comprises multiple points sampled at different instants, often at higher frequencies than the IMU. This results in motion distortion of the points within each LiDAR frame due to varying sampling times. To overcome this concern, this study introduces an interpolation-based approach, where each LiDAR point is mapped to its corresponding IMU position at the sampling moment. The interpolated points are then remapped into a standard coordinate system at a unified time, thereby mitigating distortion within the LiDAR scan frame. Specifically, the interpolation method utilizes IMU trajectory data to adjust the position of each LiDAR point, employing both spatial and temporal interpolation to align the points to a standardized time. This process effectively reduces motion aberrations caused by the temporal discrepancies between the LiDAR and IMU data.

2.3.2. State update

After the LiDAR scan data has undergone undistortion, the undistorted point cloud is used to formulate the observation residuals for system state optimization. Further details on deriving the observation residual function are outlined in section 2.4, and the system state update, which relies on (14) and (15), is presented in section 2.5. By incorporating the constraints from the undistorted point cloud data, this process adjusts the position and orientation estimates, thereby improving the accuracy of the state estimation. A key aspect of this procedure is transforming the observation information from the LiDAR scan into constraints on the position and attitude, thereby effectively integrating data from multiple sensors. This integration enhances the optimization process by leveraging complementary information and refining the system's performance.

2.3.3. Backward Kalman smoothing

After the state update, the IMU position estimates obtained during the forward propagation are refined using Kalman smoothing. This process corrects the current position estimates and utilizes past and future observation data, providing a more accurate and smooth result. The corrected IMU positions, refined through Kalman smoothing, are then used in the subsequent backward propagation step to enhance the point cloud undistortion further. The advantage of Kalman smoothing over traditional filtering is that it optimizes the system state by considering a broader range of observations, including future data, thereby improving the accuracy of the current state and enhancing overall system stability. This mutual enhancement—where the improved estimates from the smoothing phase enhance the following undistortion process, which improves the next update—creates a positive feedback loop, leading to progressively more accurate results [22].

$$x_{k+1}^{-} = f(x_k, u_k) \tag{2}$$

$$P_{k+1}^{-} = (I + F_k \Delta t) P_k (I + F_k \Delta t)^T + (C_k \Delta t) Q_k (C_k \Delta t)^T \tag{3}$$

$$G_k = P_k (I + F_k \Delta t)^T [P_{k+1}^{-}]^{-1} \tag{4}$$

$$x_k^s = x_k + G_k [x_{k+1}^s - x_{k+1}^{-}] \tag{5}$$

$$P_k^s = P_k + G_k [P_{k+1}^s - P_{k+1}^{-}] G_k^T \tag{6}$$

For the detailed forms of $f(x_k, u_k)$, F_k, C_k and Q_k, the readers can refer to [24], x_k^s and P_k^s represent the outcomes of the backward smoothing process, which is initiated from the final sub-frame at time T , with $x_T^s = x_T$ and $P_T^s = P_T$. A comprehensive description of the Kalman smoother is provided in [25]. When applying the Kalman smoothing process to the error state, certain adjustments to the backward smoothing stage are required, as presented in (2)-(6).

2.4. Adaptive covariance-based observation models

Measurement model: After the backward propagation, all LiDAR points are considered to be sampled simultaneously at the end of the scan. Let k be the LiDAR scan index and $\{ {}^L P_j, j = 1, \cdots, m \}$ the points in the k -th scan, expressed in the local LiDAR coordinate frame L at the scan end-time. Each measured point ${}^L P_j$ is affected by measurement noise ${}^L n_j$ comprising the ranging errors and beam-direction deviations. Eliminating this noise yields the true point position in the local LiDAR coordinate frame ${}^L P_j^{gt}$.

$${}^L P_j^{gt} = {}^L P_j + {}^L n_j \tag{7}$$

Once projected to the global coordinate frame using the respective LiDAR pose ${}^{G}T_{I_k} = ({}^{G}R_{I_k}, {}^{G}P_{I_k})$ and extrinsic ${}^{I}T_L$, this true point should coincide with a local planar surface in the map, i.e.,

$$0 = {}^{G}u_j^T\left({}^{G}T_{I_K}\ {}^{I}T_L\left({}^{L}p_j + {}^{L}n_j\right) - {}^{G}q_j\right) \tag{8}$$

where ${}^{G}u_j$ denotes the plane's normal vector and ${}^{G}q_j$ represents a point located on that plane in Figure 3. Both ${}^{G}T_{I_k}$ and ${}^{I}T_{L_k}$ are components of the state vector X_k. Hence, the measurement for the j -th point ${}^{L}p_j$ can be simplified from (8) into the compact expression:

$$0 = h_j\left(x_k, {}^{L}p_j + {}^{L}n_j\right) \tag{9}$$

which implicitly defines the measurement model for the state vector X_k.

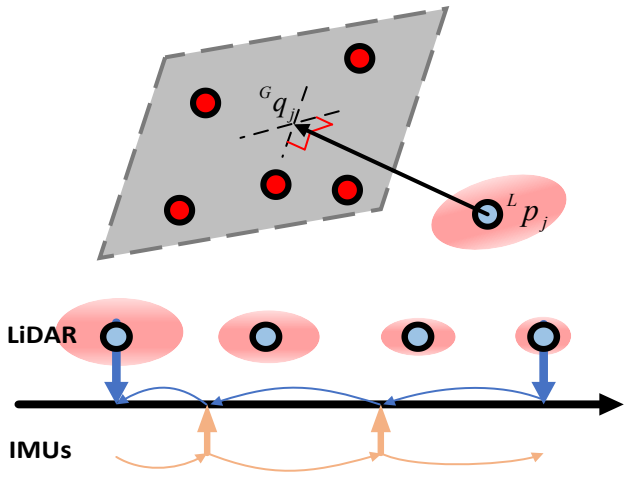

Figure 3. Observation models

Unlike FAST-LIO2, which assumes that all points in the point cloud have the same confidence level, this paper considers that intense sensor motion and significant de-distortion time differences often degrade point cloud accuracy. Therefore, this paper proposes an adaptive error covariance computation scheme based on the intensity of IMU motion and the de-alignment time difference, which dynamically adjusts the error weights in the point cloud. The proposed strategy enhances the overall accuracy of the LIO system, as detailed in the process presented below.

First, the motion intensity of the sensor is characterized by the acceleration and angular velocity of the IMU. Let the acceleration paradigm of the IMU at moment t_i be $|a(t_i)|$, and the angular velocity paradigm be $|\omega(t_i)|$. Then, the motion intensity can be expressed as:

$$M_i = \alpha\left|a\left(t_i\right)\right| + \beta\left|\omega\left(t_i\right)\right| \tag{10}$$

where α and β are weighting coefficients regulating the relative influence of acceleration and angular velocity on the error. The more violent the sensor's motion, the greater the motion intensity M_i and the corresponding point cloud error.

Second, consider the effect of the de-distortion time difference. For point p_i, whose acquisition moment is t_i and the current moment is t_{curr}, the time difference $\Delta t = t_{curr} - t_i$ reflects the lag degree of the de-distortion process. As the time difference increases, the error in the de-distortion process gradually accumulates, expressed as:

$$T_i = \gamma\Delta t \tag{11}$$

where γ is the time lag error coefficient, which measures the contribution of the time lag to the error.

Based on the above two factors, M_i and Ti, the covariance matrix $\sum i$ for each point Pi in the point cloud can be expressed as:

$$\sum i = \sigma_0^2 (M_i + T_i) I \tag{12}$$

where σ_0^2 denotes the underlying noise variance and I is the unit matrix, which indicates that the error characteristics are consistent in all directions. This adaptive covariance model enables the LIO system to dynamically adjust the confidence level of different points based on the error characteristics of the point cloud data. Specifically, point clouds with more significant errors (e.g., points with high motion intensity or considerable time difference) will receive lower confidence levels, thus weakening their impact on the system state estimation. In contrast, high-quality point clouds will increase their contribution to the system state estimation by enhancing the constraints.

This adaptive covariance method effectively enhances the robustness and accuracy of the LIO system in complex dynamic environments, particularly in cases where sensor motion is violent, and the quality of point cloud data is uneven, allowing for the more effective utilization of valuable information and mitigating the negative impact of low-quality data on system performance.

2.5. Kalman update

The point-to-plane residuals formulated in (9) are employed as measurement inputs for the iterative Kalman state update:

$$K = (H^T R^{-1} H + P_k^{-1})^{-1} H^T R^{-1} \tag{13}$$

$$x_k^{K+1} = x_k^K + K\left(0 - h(x_k^K)\right) - (I - KH)(x_k^K - x_k^0) \tag{14}$$

where H denotes the Jacobian matrix of the measurement model, reflecting the sensitivity of the residuals to state variations, and R represents the measurement noise covariance, which models the uncertainty in the observed measurements. The updated nominal state x_k^{K+1} is iteratively updated by correcting the predicted state x_k^0 using the Kalman gain K and the residual between the measurement model $h(x_k^K)$ and the actual observations.

During each iteration, the nominal state was corrected, and the error state was reset. When the iterations converged, the state covariance was updated using (15):

$$P_k = (I - KH) P_k \tag{15}$$

IMU data were then used for nominal state prediction via a discrete-time propagation model:

$$x_{k+1} = f(x_k, u_k) \tag{16}$$

The linearized discrete-time error-state transition in Eq. (17) was applied to propagate the error-state covariance forward, as expressed in (18).

$$\delta x_{k+1} = (I + F_k \Delta t)\delta x_k + (C_k \Delta t)\omega \tag{17}$$

$$P_{k+1} = (I + F_K \Delta t) P_k (I + F_k \Delta t)^T + (C_k \Delta t) Q_k (C_k \Delta t)^T \tag{18}$$

The outcome of this forward propagation was then applied for motion compensation and registration.

3. RESULTS AND DISCUSSION

To validate the performance of our proposed method, it is compared with Fast-LIO2 [19], Faster-LIO [20], Point-LIO [21], and FR-LIO [22] on nine sequences of the publicly available NTU-VIRAL dataset [23]. Figures 4 to 5 depict the mapping and simulation results of ADC-LIO in different dataset sequences. NTU-VIRAL data integrates diverse sensor configuration, including two 3D LIDARs, dual time-synchronized cameras, multiple IMUs, and four sets of ultra-wideband (UWB) nodes, to form an all-encompassing sensing system for the complex requirements of autopiloted vehicles. Through

flight testing in various indoor and outdoor environments, NTU VIRAL has captured high-quality multimodal data. The technical highlight of this dataset is its unique and detailed sensor integration scheme, which mimics the sensor configuration of an autonomous vehicle but exhibits more complex challenges and characteristics in an airborne application.

Table 1 presents the experimental findings of the developed ADC-LIO and current state-of-the-art (SOTA) LiDAR-inertial odometry systems on the nine sequences, i.e., eee_01 to _03, nya_01 to _03, and sbs_01 to _03, of the NTU-VIRAL dataset. The performance is evaluated based on the Absolute Position Errors (APE), indicating that ADC-LIO achieves the slightest absolute error across all sequences. This improvement is due to our system considering the impact of motion distortion on pose estimation through adaptive covariance, which enhances the influence of points with low distortion and high accuracy during the pose estimation process, thereby increasing the overall system precision. Overall, ADC-LIO achieves an APE of approximately 50%, ranking as the second-best performing method, which demonstrates that the proposed method demonstrates superior performance compared to existing SOTA approaches.

Table 1. Absolute position errors in NTU-VIRAL dataset with different algorithms

Algorithm	Sequence								
	eee_01	eee_02	eee_03	nya_01	nya_02	nya_03	sbs_01	sbs_02	sbs_03
Fast-LIO2 [19]	0.1350	0.1180	0.1640	0.1210	0.1400	0.1500	0.1440	0.1440	0.1320
Faster-LIO [20]	0.1440	0.1210	0.1620	0.1320	0.1720	0.1540	0.1440	0.1440	0.1340
Point-LIO [21]	0.1950	0.1300	0.1820	0.1820	0.1640	0.1900	0.1970	0.2140	0.1890
FR-LIO [22]	0.1320	0.1180	0.1640	0.1200	0.1390	0.1470	0.1440	0.1430	0.1320
ADC-LIO	**0.0757**	**0.0682**	**0.1143**	**0.0595**	**0.0910**	**0.1109**	**0.0896**	**0.0769**	**0.0775**

Figure 4 visualizes the corresponding experimental results of ADC-LIO. The first row illustrates the estimated trajectories represented by blue curves alongside the dense 3D point clouds generated by ADC-LIO for the eee_01, nya_01, and sbs_01 sequences. The point clouds are color-coded according to the intensity information of each point, highlighting our method's capability to preserve fine details. The high precision of the pose estimation results in minimal ghosting effects in the dense point clouds, thereby effectively capturing the intricate structures of the surrounding environment. Additionally, the second row depicts the estimated trajectories alongside the APE metric, where the gray dashed lines represent the ground truth. The trajectories are color-coded to reflect varying magnitudes of error, providing a clear visual representation of the algorithm's accuracy relative to the true trajectory.

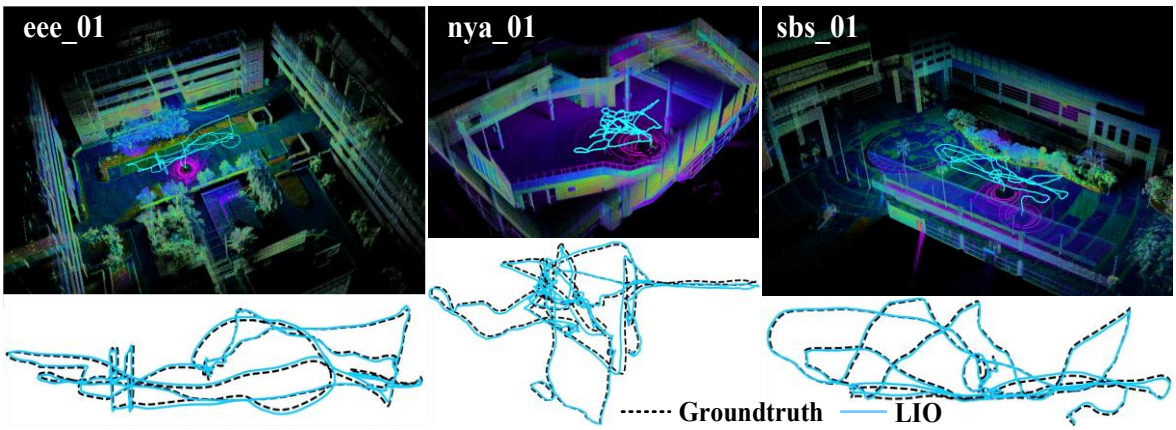

Figure 4. ADC-LIO mapping results under NTU-VIRAL sequences

Figure 5 illustrates the localization and mapping results of sequence eee_01. Specifically, Figure 5(a) explicitly illustrates the proposed algorithm's localization and mapping results for the eee_01 sequence. Figures 5(b) and 5(d) visualize the high-quality reconstruction results for non-structural, complex objects, such as trees, while Figures 5(c) and 5(e) demonstrate the reconstruction results for structured objects, such as buildings. These high-quality reconstructions are directly derived from the iterative backpropagation method proposed in this paper, significantly enhancing the quality of point cloud

undistortion. The adaptive distortion covariance also enhances the system's localization accuracy, resulting in more accurate point cloud reconstruction with reduced ghosting artifacts.

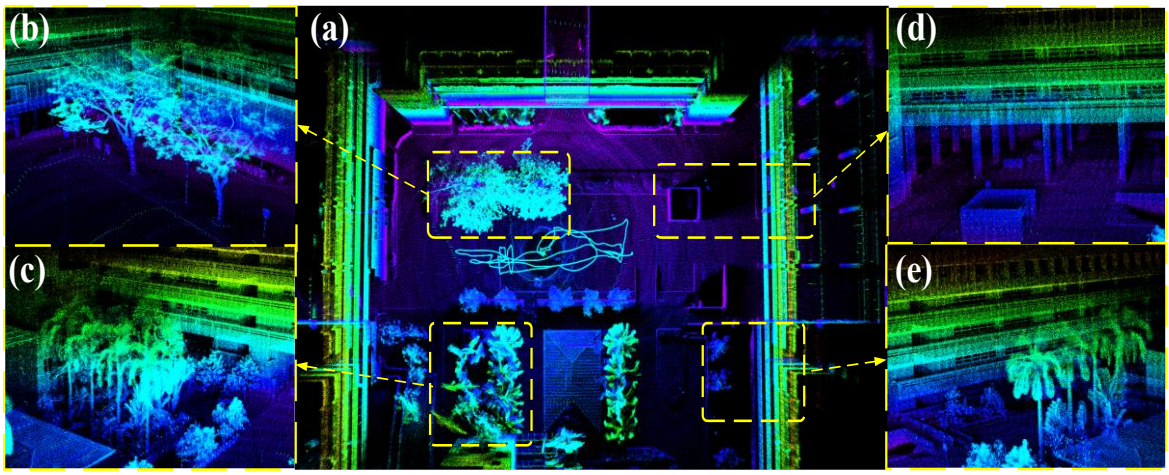

Figure 5. Localization and mapping results of sequence eee_01: (a) overall 3D reconstruction, (b) vegetation mapping, (c) mixed vegetation–structure region, (d) building façade reconstruction, and (e) structured object details

4. CONCLUSION

This paper proposes ADC-LIO, an accurate and robust LiDAR inertial odometry framework that utilizes an iterative error Kalman framework and an iterative backpropagation strategy to effectively integrate the point cloud de-distortion processing with the Kalman filter update process. The proposed method directly addresses the motion distortion challenges of mobile robots during high-speed navigation and aggressive maneuvers. In addition, ADC-LIO incorporates an adaptive covariance processing method to further enhance the constraints of high-quality point clouds. ADC-LIO is evaluated on nine sequences from the publicly available NTU-VIRAL dataset, which involves both indoor environments with significant rotational speeds and outdoor environments. The tests demonstrated that ADC-LIO produces accurate and reliable map-building results, affording an improved pose estimation accuracy compared to other SOTA approaches, including FAST-LIO, Faster-LIO, Point-LIO, and FR-LIO. In forthcoming studies, we intend to conduct a more in-depth analysis of variable covariance, aiming to improve the performance of LIO in challenging robotic scenarios such as long-term autonomous exploration and multi-robot collaborative mapping.

FUNDING INFORMATION

Authors state no funding involved.

AUTHOR CONTRIBUTIONS STATEMENT

This journal uses the Contributor Roles Taxonomy (CRediT) to recognize individual author contributions, reduce authorship disputes, and facilitate collaboration.

Name of Author	C	M	So	Va	Fo	I	R	D	O	E	Vi	Su	P	Fu
Lixiao Yang	✓	✓	✓		✓		✓	✓	✓		✓		✓	
Youbing Feng				✓		✓				✓		✓		

C : **C**onceptualization
M : **M**ethodology
So : **So**ftware
Va : **Va**lidation
Fo : **Fo**rmal analysis
I : **I**nvestigation
R : **R**esources
D : **D**ata Curation
O : Writing - **O**riginal Draft
E : Writing - Review & **E**diting
Vi : **Vi**sualization
Su : **Su**pervision
P : **P**roject administration
Fu : **Fu**nding acquisition

CONFLICT OF INTEREST STATEMENT

Authors state no conflict of interest.

DATA AVAILABILITY

Derived data supporting the findings of this study are available from the corresponding author [Feng Y] on request.

REFERENCES

[1] A. Li, J. Wang, M. Xu, and Z. Chen, "DP-SLAM: A visual SLAM with moving probability towards dynamic environments," *Information Sciences*, vol. 556, pp. 128–142, May 2021, doi: 10.1016/j.ins.2020.12.019.

[2] C. Campos, R. Elvira, J. J. G. Rodriguez, J. M. M. Montiel, and J. D. Tardos, "ORB-SLAM3: An accurate open-source library for visual, visual–inertial, and multimap SLAM," *IEEE Transactions on Robotics*, vol. 37, no. 6, pp. 1874–1890, Dec. 2021, doi: 10.1109/TRO.2021.3075644.

[3] G. Peng, Z. Lu, S. Chen, D. He, and L. Xinde, "Pose estimation based on wheel speed anomaly detection in monocular visual-inertial SLAM," *IEEE Sensors Journal*, vol. 21, no. 10, pp. 11692–11703, May 2021, doi: 10.1109/JSEN.2020.3011945.

[4] C. Yan *et al.*, "GS-SLAM: Dense visual SLAM with 3D Gaussian splatting," in *Proceedings of the IEEE Computer Society Conference on Computer Vision and Pattern Recognition*, Jun. 2024, pp. 19595–19604, doi: 10.1109/CVPR52733.2024.01853.

[5] H. Wang, C. Wang, C.-L. Chen, and L. Xie, "F-LOAM: Fast LiDAR odometry and mapping," in *2021 IEEE/RSJ International Conference on Intelligent Robots and Systems (IROS)*, Sep. 2021, pp. 4390–4396, doi: 10.1109/IROS51168.2021.9636655.

[6] J. Levinson and others, "Towards fully autonomous driving: Systems and algorithms," in *2011 IEEE Intelligent Vehicles Symposium (IV)*, Jun. 2011, pp. 163–168, doi: 10.1109/IVS.2011.5940562.

[7] C. Badue and others, "Self-driving cars: A survey," *Expert Systems with Applications*, vol. 165, p. 113816, Mar. 2021, doi: 10.1016/j.eswa.2020.113816.

[8] S. Liu and others, "Planning dynamically feasible trajectories for quadrotors using safe flight corridors in 3-D complex environments," *IEEE Robotics and Automation Letters*, vol. 2, no. 3, pp. 1688–1695, Jul. 2017, doi: 10.1109/LRA.2017.2663526.

[9] A. Mokhtari, A. Benallegue, and Y. Orlov, "Exact linearization and sliding mode observer for a quadrotor unmanned aerial vehicle," *International Journal of Robotics and Automation*, vol. 21, no. 1, pp. 39–49, 2006, doi: 10.2316/Journal.206.2006.1.206-2842.

[10] C. Yuan, W. Xu, X. Liu, X. Hong, and F. Zhang, "Efficient and probabilistic adaptive voxel mapping for accurate online LiDAR odometry," *IEEE Robotics and Automation Letters*, vol. 7, no. 3, pp. 8518–8525, Jul. 2022, doi: 10.1109/LRA.2022.3187250.

[11] Y. Pan, P. Xiao, Y. He, Z. Shao, and Z. Li, "MULLS: Versatile LiDAR SLAM via multi-metric linear least square," in *2021 IEEE International Conference on Robotics and Automation (ICRA)*, May 2021, pp. 11633–11640, doi: 10.1109/ICRA48506.2021.9561364.

[12] G. Chen, B. Wang, X. Wang, H. Deng, B. Wang, and S. Zhang, "PSF-LO: Parameterized semantic features based lidar odometry," in *2021 IEEE International Conference on Robotics and Automation (ICRA)*, May 2021, pp. 5056–5062, doi: 10.1109/ICRA48506.2021.9561554.

[13] J.-E. Deschaud, "IMLS-SLAM: Scan-to-model matching based on 3D data," in *2018 IEEE International Conference on Robotics and Automation (ICRA)*, May 2018, pp. 2480–2485, doi: 10.1109/ICRA.2018.8460653.

[14] P. Dellenbach, J.-E. Deschaud, B. Jacquet, and F. Goulette, "CT-ICP: Real-time elastic LiDAR odometry with loop closure," in *2022 International Conference on Robotics and Automation (ICRA)*, May 2022, pp. 5580–5586, doi: 10.1109/ICRA46639.2022.9811849.

[15] J. Lv, K. Hu, J. Xu, Y. Liu, X. Ma, and X. Zuo, "CLINS: Continuous-time trajectory estimation for LiDAR-inertial system," in *2021 IEEE/RSJ International Conference on Intelligent Robots and Systems (IROS)*, Sep. 2021, pp. 6657–6663, doi: 10.1109/IROS51168.2021.9636676.

[16] T. Shan, B. Englot, D. Meyers, W. Wang, C. Ratti, and D. Rus, "LIO-SAM: Tightly-coupled lidar inertial odometry via smoothing and mapping," in *2020 IEEE/RSJ International Conference on Intelligent Robots and Systems (IROS)*, Oct. 2020, pp. 5135–5142, doi: 10.1109/IROS45743.2020.9341176.

[17] K. Chen, R. Nemiroff, and B. T. Lopez, "Direct LiDAR-inertial odometry: Lightweight LIO with continuous-time motion correction," in *2023 IEEE International Conference on Robotics and Automation (ICRA)*, May 2023, pp. 3983–3989, doi: 10.1109/ICRA48891.2023.10160508.

[18] W. Xu and F. Zhang, "FAST-LIO: A fast, robust LiDAR-inertial odometry package by tightly-coupled iterated Kalman filter," *IEEE Robotics and Automation Letters*, vol. 6, no. 2, pp. 3317–3324, Apr. 2021, doi: 10.1109/LRA.2021.3064227.

[19] W. Xu, Y. Cai, D. He, J. Lin, and F. Zhang, "FAST-LIO2: Fast direct LiDAR-inertial odometry," *IEEE Transactions on Robotics*, vol. 38, no. 4, pp. 2053–2073, Aug. 2022, doi: 10.1109/TRO.2022.3141876.

[20] C. Bai, T. Xiao, Y. Chen, H. Wang, F. Zhang, and X. Gao, "Faster-LIO: Lightweight tightly coupled lidar-inertial odometry using parallel sparse incremental voxels," *IEEE Robotics and Automation Letters*, vol. 7, no. 2, pp. 4861–4868, Apr. 2022, doi: 10.1109/LRA.2022.3152830.

[21] D. He, W. Xu, N. Chen, F. Kong, C. Yuan, and F. Zhang, "Point-LIO: Robust high-bandwidth light detection and ranging inertial odometry," *Advanced Intelligent Systems*, vol. 5, no. 7, p. 2200459, Jul. 2023, doi: 10.1002/aisy.202200459.

[22] J. Liu, Y. Zhang, X. Zhao, Z. He, W. Liu, and X. Lv, "Fast and robust LiDAR-inertial odometry by tightly-coupled iterated Kalman smoother and robocentric voxels," *IEEE Transactions on Intelligent Transportation Systems*, vol. 25, no. 10, pp. 14486–14496, Oct. 2024, doi: 10.1109/TITS.2024.3391291.

[23] T.-M. Nguyen, S. Yuan, M. Cao, Y. Lyu, T. H. Nguyen, and L. Xie, "NTU VIRAL: A visual-inertial-ranging-lidar dataset, from an aerial vehicle viewpoint," *The International Journal of Robotics Research*, vol. 41, no. 3, pp. 270–280, Mar. 2022, doi: 10.1177/02783649211052312.

[24] J. Solà, "Quaternion kinematics for the error-state Kalman filter." Nov. 2017, doi: 10.48550/arXiv.1711.02508.

[25] S. Särkkä, *Bayesian filtering and smoothing*. Cambridge, UK: Cambridge University Press, 2013.

BIOGRAPHIES OF AUTHORS

Lixiao Yang received the B.E. degree from Jiangsu University of Science and Technology, Zhenjiang, China, in 2023. He is currently working toward the M.S. degree with the Ocean College, Jiangsu University of Science and Technology, Zhenjiang, China. His research interests include slam and sensor fusion. He can be contacted at 13052750039@163.com.

Youbing Feng (CCF Member) received the B.E. degree from Suzhou University, Suzhou, China, in 2000. and the Ph.D. degree from Jiangsu University, Zhenjiang, China, in 2009. He is currently an assistant professor with Ocean College, Jiangsu University of Science and Technology. His research interests include agricultural internet of things, wireless sensor network and control of UAVS. He can be contacted at yzfyb@just.edu.cn.